Parker & Jefferson, 1982; Price & Parker, 1984). Such an investigation is in progress.

We should like to encourage experimentalists to test the ideas presented in this paper by obtaining more experimental results on the phase diagrams of polytypic compounds as a function of temperature and pressure. Data are at present scarce due to the difficulties imposed by the inevitable presence of defects which are known to affect strongly the stability of polytypic phases.

We should like to thank Desmond McConnell, Volker Heine, Jonathan Smith and Heinrich Röder for many useful ideas and discussions. GDP gratefully acknowledges the receipt of a Royal Society Research Fellowship.

References

AKAOGI, M., AKIMOTO, S., HORIOKA, K., TAKAHASHI, K. & HORIUCHI, H. (1982). *J. Solid State Chem.* **44**, 257–267.
AKAOGI, M. & NAVROTSKY, A. (1984). *Phys. Chem. Miner.* In the press.
BAK, P. (1982). *Rep. Prog. Phys.* **45**, 587–629.
BAK, P. & VON BOEHM, J. (1980). *Phys. Rev. B*, **21**, 5297–5308.
CATLOW, C. R. A., THOMAS, J. M., PARKER, S. C. & JEFFERSON, D. A. (1982). *Nature (London)*, **295**, 658–662.
DAVIES, P. K. & AKAOGI, M. (1983). *Nature (London)*, **305**, 788–790.
DEER, W. A., HOWIE, R. A. & ZUSSMAN, J. (1978). *Rock Forming Minerals.* 1*A*. London: Longman.
DUXBURY, P. M. & SELKE, W. (1983). *J. Phys. A Gen. Phys.* **16**, L741–L744.
ELLIOTT, R. J. (1961). *Phys. Rev.* **124**, 346–353.
FISHER, M. E. & SELKE, W. (1980). *Phys. Rev. Lett.* **44**, 1502–1505.
FISHER, M. E. & SELKE, W. (1981). *Philos. Trans. R. Soc. London*, **302**, 1–44.
FRANK, F. C. (1951). *Philos. Mag.* **42**, 1014–1021.
HAZEN, R. M. & FINGER, L. W. (1981). *Structure and Bonding in Crystals.* II, edited by M. O'KEEFFE & A. NAVROTSKY, pp. 109–118. New York: Academic Press.
HENMI, C., KAWAHARA, A., HENMI, K., KUSACHI, I. & TAKEUCHI, Y. (1983). *Am. Mineral.* **68**, 156–163.
HORIUCHI, H., AKAOGI, M. & SAWAMOTO, H. (1982). *Adv. Earth Planet. Sci.* **12**, 391–403.
HORIUCHI, H., HORIOKA, K. & MORIMOTO, N. (1980). *J. Mineral. Soc. Jpn*, **2**, 253–264.
HYDE, B. G., WHITE, T. J., O'KEEFFE, M. & JOHNSON, A. W. S. (1982). *Z. Kristallogr.* **160**, 53–62.
IIJIMA, S. & BUSECK, P. R. (1975). *Am. Mineral.* **60**, 758–770.
JAGODZINSKI, H. (1954). *Neues Jahrb. Mineral. Monatsh.* **3**, 49–65.
JEPPS, N. W. & PAGE, T. F. (1983). *J. Cryst. Growth Charact.* **7**, 259–307.
LANDAU, L. D. & LIFSHITZ, E. M. (1958). *Statistical Physics.* London: Pergamon.
MA, C. B. (1974). *Contrib. Mineral. Petrol.* **45**, 257–279.
PRICE, G. D. (1983). *Phys. Chem. Miner.* **10**, 77–83.
PRICE, G. D. & PARKER, S. C. (1984). *Phys. Chem. Miner.* **10**, 209–216.
SMITH, J., YEOMANS, J. & HEINE, V. (1984). *Proceedings of NATO Advanced Studies Institute on Modulated Structure Materials*, edited by T. TSAKALAKOS. In the press.
THOMPSON, J. B. (1978). *Am. Mineral.* **63**, 239–249.
THOMPSON, J. B. (1981). *Structure and Bonding in Crystals.* II, edited by M. O'KEEFFE & A. NAVROTSKY, pp. 167–188. New York: Academic Press.
TRIGUNAYAT, G. C. & CHADHA, G. K. (1971). *Phys. Status Solidi A*, **4**, 9–42.
WELTNER, W. (1969). *J. Chem. Phys.* **51**, 2469–2483.
WHITE, T. J. & HYDE, B. G. (1983). *Acta Cryst.* B**39**, 10–17.
ZEN, E. (1967). *Am. Mineral.* **52**, 635–660.

Acta Cryst. (1984). B**40**, 454–461

Use of Dynamical Scattering in the Structure Determination of a Minute Fluorocarbonate Mineral Cebaite $Ba_3Ce_2(CO_3)_5F_2$ by High-Resolution Electron Microscopy

BY F. H. LI

Institute of Physics, Academia Sinica, Beijing, China

AND H. HASHIMOTO

Department of Applied Physics, Osaka University, Suita, Osaka 565, *Japan*

(*Received* 11 *January* 1984; *accepted* 16 *March* 1984)

Abstract

A method for determining the crystal structure using the dynamical extinction effect in the electron diffraction appearing in high-resolution electron micrographs is proposed for the mineral cebaite $Ba_3Ce_2(CO_3)_5F_2$ whose heavy-atom positions have not previously been determined but only estimated. The specimen is thicker than the maximum thickness for which the weak-phase-object approximation is applicable, so that the extinction effect becomes predominant and the image contrast of light atoms is enhanced. Using electron micrographs of huanghoite $BaCe(CO_3)_2F$, whose atomic structure is known and related to that of cebaite, the optimum thickness and imaging condition, which can reveal the image of light atoms as well as heavy atoms, are investigated. The optimum thickness is found to be 45 to 50 Å

0108-7681/84/050454-08$01.50

and the optimum underfocus is about 400 Å. Under these conditions the image contrast of light atoms is enhanced and both the heavy and light atoms are revealed with sufficient contrast. For cebaite the optimum conditions are 50 Å in thickness and 450 Å for the underfocus value. By matching the theoretical and observed contrasts in the images the positions of light atoms are determined together with those of the heavy atoms. It is found that the optimum thickness has a value larger than the thickness where the amplitude of the strongest diffracted beam has its maximum value. This thickness, however, is not much larger than the value at which the amplitude of the strongest diffracted beam becomes smaller than that of the weak beams.

1. Introduction

Recently, high-resolution electron microscopy (HREM) has become a useful technique to determine crystal structure (Sundberg, 1978–79; O'Keefe, Buseck & Iijima, 1978; Kumao, Hashimoto, Nissen & Endoh, 1981). Some crystals, including both natural and synthetic ones, are very small, and the area of uniform structure is limited to regions of about one hundred ångströms in diameter or even smaller, and it is not possible to get homogeneous single crystals large enough for X-ray diffraction analysis. For instance, a new barium cerium fluorocarbonate mineral cebaite with formula $Ba_3Ce_2(CO_3)_5F_2$ is exclusively found in paragenesis with other alkaline-earth cerium fluorocarbonate minerals (Li, Fan, Zhang & Wang, 1983; Li & Fan, 1982*a*) and its size is a few hundred ångströms. Therefore, cebaite is a good test example for structure determination by HREM. So far only a hypothetical structure model of cebaite has been proposed by Peng & Shen (1979) on the basis of crystal chemical considerations. The present paper is concerned with the determination of the crystal structure of cebaite by HREM. It is important for the present problem that the new mineral contains both very heavy atoms, *i.e.* barium and cerium, and light atoms, *i.e.* carbon, oxygen and fluorine.

In general, a very thin crystal can be treated as a weak phase object and the contrast of heavy atoms in the structure image will be higher than that of the light atoms (Cowley & Iijima, 1972; Kumao, Hashimoto, Nissen & Endoh, 1981). Carbon, oxygen and fluorine atoms have much weaker scattering power than barium and cerium atoms, and so the contribution of light atoms to the image contrast is negligibly small compared to that of barium and cerium. Accordingly, in order to derive structural information about the light atoms from a high-resolution image it is desirable to obtain the image from a not too thin crystal. This may enhance the contrast of the light atoms, so that both heavy and light atoms may be revealed with sufficient contrast. Besides depending on the crystal thickness, the image contrast is also related to the imaging conditions, especially to the defocus value. However, it is difficult to determine the optimum crystal thickness and the optimum defocus value for the case of cebaite with an unknown crystal structure. In such a case, it is advantageous to investigate the structure image of huanghoite $BaCe(CO_3)_2F$, a mineral which belongs to the same family as cebaite, whose crystal structure is already known (Semionov & Zhang, 1961; Fan, Zhang & Zhao, 1963; Qian, Fu, Kong & Gong, 1982). Structure images of huanghoite were therefore taken in order to find the optimum thickness and the optimum defocus where a high image contrast is found at the positions of the light atoms.

2. Crystal structure and image simulation

Both huanghoite and cebaite can be assumed to have the same basic structure if the light atoms, carbon, oxygen and fluorine, are ignored and the heavy atoms, barium and cerium, are assumed to have the same scattering amplitude. The subcell is hexagonal with parameters $a_0 = 5{\cdot}07$, $c_0 = 9{\cdot}52$ Å for huanghoite and $a_0 = 5{\cdot}06$, $c_0 = 9{\cdot}63$ Å for cebaite (Li & Fan, 1982*b*). However, these two minerals are different in superstructure. Huanghoite belongs to the trigonal system and the hexagonal unit cell is four times as large as the subcell with lattice parameters $a = 5{\cdot}06$ and $c = 38{\cdot}08$ Å (Li, Fan, Yang, Fu & Kong, 1982), while cebaite is monoclinic with lattice parameters $a = 21{\cdot}2$, $b = 5{\cdot}06$, $c = 13{\cdot}1$ Å and $\beta = 95°$ (Li & Fan, 1982*b*). For both crystals, images projected along the b axis are most advantageous for viewing their crystal structures. Fig. 1 shows a projection of the crystal structure model of huanghoite and the projection of the heavy atoms in the hypothetical structure model of cebaite proposed earlier, along the b axis. Theoretical images were calculated by the multislice method (Cowley & Moodie, 1957). The beam divergence and the defocus distribution caused by the chromatic aberration were not taken into consideration, because they were about 0·1 mrad and 100 Å respectively (Takai, Hashimoto, Endoh & Ajika, 1981). The images were calculated by changing the crystal thickness in steps of 5–10 Å and the defocus in steps of 50 Å from image to image.

3. Experimental

Minute fragments of the minerals were crushed in an agate mortar. The powder was dispersed in acetone and transferred to copper grids coated with holey carbon films. These specimens were examined at 100 kV with a JEM 100 C microscope equipped with a high-resolution top-entry goniometer. The spherical aberration coefficient of the objective lens is 0·7 mm. Several through-focus series of images were taken without objective aperture. The crystallites were tilted

up to ±10° so as to make the *b* axis parallel to the incident beam for both kinds of mineral specimens. Huanghoite and cebaite are generally cloven along planes different from the (010) plane. The probability of getting a crystal fragment in the desired orientation by tilting less than 10° is very small. Furthermore, the crystals were so easily damaged under the strong electron beam irradiation that the images were taken under a weak incident beam.

4. Images of huanghoite

Figs. 2(*a*), (*b*) and (*c*) show three observed images from a through-focus series taken with 100 Å defocus steps, together with the corresponding calculated images for an assumed specimen thickness of 50 Å and underfocus values of 300, 400 and 500 Å, respectively. The resolution of the images is about 3 Å. The contrast of the images changes drastically from image to image. However, by comparing the atomic structure model, it can be seen that the best correspondence of the image with the crystal structure appears in the image shown in Fig. 2(*b*). In this image, all the atoms, light as well as heavy, appear dark and have sufficient contrast. The correspondence can be seen more clearly in Fig. 3, where the image calculated for crystal thickness of 50 Å and underfocus of 400 Å is superimposed on the projected structure model of huanghoite along the *b* axis. All the atoms appear in dark contrast. The white dots correspond to regions surrounded by columns of heavy atoms as well as light atoms. All the white dots are arranged in horizontal lines, but they are in a zigzag line in the direction indicated by

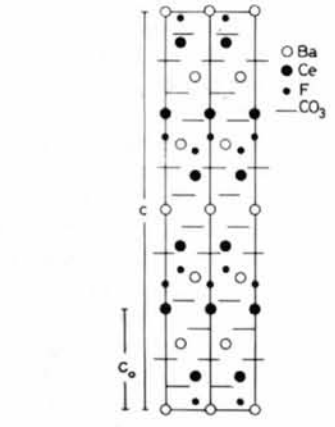

(*a*)

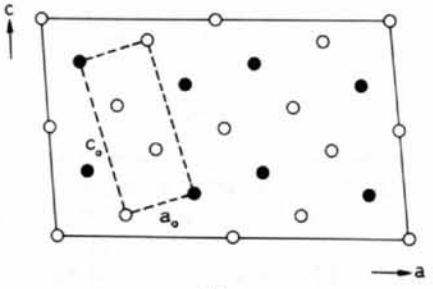

(*b*)

Fig. 1. Projection of (*a*) the structure model of huanghoite and (*b*) the approximate structure model of cebaite along *b* axis. a_0 and c_0 represent parameters of the subcell.

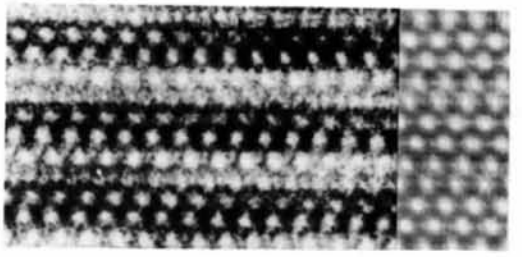

(*a*)

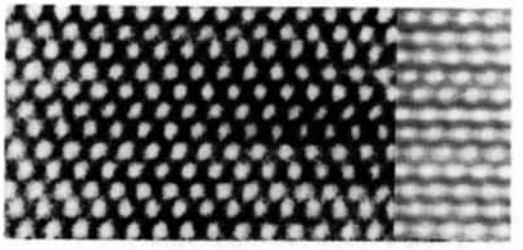

(*b*)

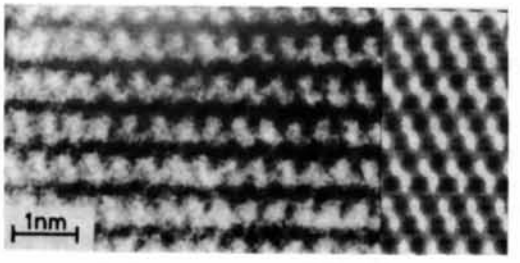

(*c*)

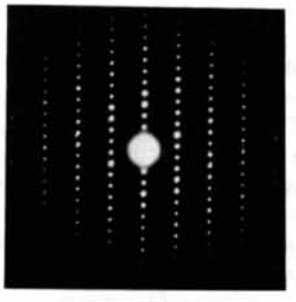

(*d*)

Fig. 2. Observed and calculated images of huanghoite for crystal thickness 50 Å, spherical aberration coefficient 0·7 mm and underfocus (*a*) 300 Å, (*b*) 400 Å and (*c*) 500 Å. (*d*) Corresponding electron diffraction pattern. Incident beam is parallel to the *b* axis.

arrows labelled *A* and *B*. This cannot be explained by considering only the arrangement of heavy atoms which line up along the horizontal and in the directions *A* and *B*. However, the light atoms are arranged in the straight horizontal lines and in the zigzag lines in the directions *A* and *B*. This means that the contribution of light atoms to the image at a thickness of 50 Å and an underfocus of 400 Å is rather strong compared to that of the heavy atoms. This image is very useful for extracting information about the position of the light atoms.

5. Optimum image formation condition

According to the image simulation for huanghoite the contribution of light atoms to the image formation would be enhanced if the crystal thickness were about 45–50 Å, where the light atoms could reveal themselves in the image with sufficient dark contrast. This can be interpreted in the following way. Table 1 gives the ordinary structure factors F of huanghoite and the structure factors F' calculated by assuming that huanghoite consists of heavy atoms only. The indices of the three strongest diffracted beams are marked by asterisks. Comparison of F and F' shows that for strong reflections the real part of the structure factor does not change much and the imaginary part retains its sign unchanged even when the light atoms are discarded. However, for weak reflections both the real and imaginary parts of the structure factor change a lot and the imaginary part even changes sign. This indicates that the strong diffracted beams are contributed to mainly by the heavy atoms, while the weak beams are contributed to mainly by the light atoms. Fig. 4 shows the dependence of the amplitude of the diffracted beams on the crystal thickness in huanghoite. The amplitudes of the three strongest beams with indices 108, $10\bar{4}$ and 0,0,12 increase with increasing thickness at first, but after arriving at certain maximum values they decrease with increasing thickness, while the amplitudes of weak diffracted beams with indices 003, 006 and $10\bar{1}$ increase with increasing thickness monotonically. By combining Table 1 and Fig. 4 it can be concluded that the proportion of the contribution of light atoms to that of heavy atoms in the image contrast increases with the crystal thickness. Furthermore, after the amplitude of the strongest diffracted beam 108 reaches its maximum value at 30 Å the information of heavy atoms transferred to the image is decreased and the influence of light atoms increases. Therefore, it could be expected that the optimum thickness which is most advantageous for

Table 1. *Structure image of huanghoite*

hkl	F_{Re}	F'_{Re}	F_{Im}	F'_{Im}
003	0·088	0·336	0·017	−0·031
006	−0·972	−0·007	−0·041	0·030
$10\bar{1}$	−0·185	−0·095	0·268	0·009
102	0·102	−0·057	0·049	0·009
009	−1·368	−0·832	−0·275	−0·094
*$10\bar{4}$	3·201	5·702	−0·364	−0·054
105	−0·436	−0·447	−0·180	−0·047
$10\bar{7}$	1·210	0·595	0·245	0·051
*108	6·078	5·080	0·360	0·096
*0,0,12	2·465	4·926	0·131	0·140

F structure factor of huanghoite.
F' structure factor taking only heavy atoms of huanghoite into account.
Re real part, Im imaginary part.

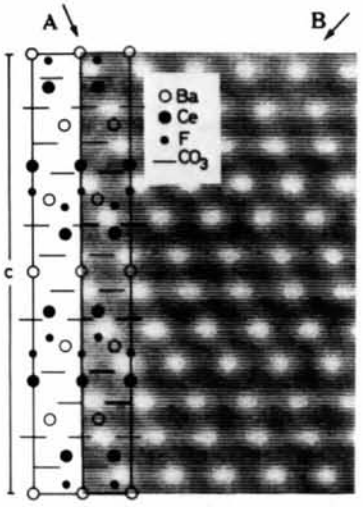

Fig. 3. Calculated image and corresponding structure model of huanghoite projected along the *b* axis. Crystal thickness is 50 Å, spherical aberration coefficient 0·7 mm and underfocus 400 Å.

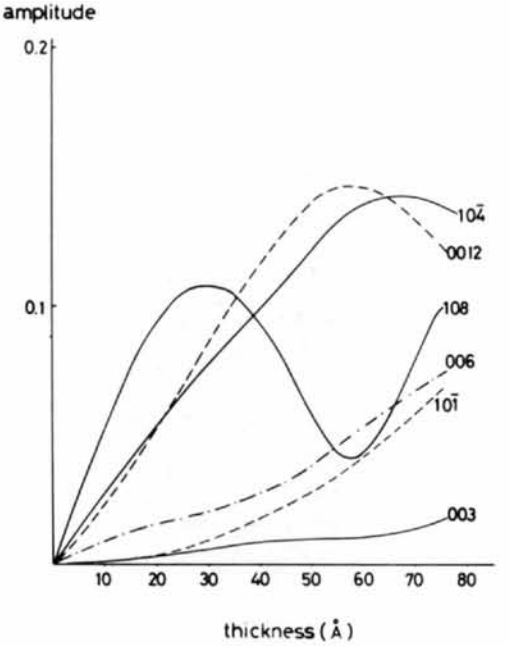

Fig. 4. Variation of the amplitude of diffracted beams with thickness in huanghoite.

revealing both the light and heavy atoms in the image would have a value larger than the thickness where the amplitude of the strongest diffracted beam reaches its maximum value, but not larger than the thickness at which the amplitude of the strongest beam becomes smaller than those of weak beams. For example, if the thickness of the crystal is larger than 50 Å, say 60 Å, the image contrast does not correspond to the crystal structure. The calculated contrast of the image of huanghoite with 63 Å thickness is shown in Fig. 5 together with the projection of the structure model. In Fig. 5, cerium atoms appear dark, while barium atoms appear bright, which suggests that 63 Å is not adequate to reveal the images of both light and heavy atoms correctly. Thus, for huanghoite the optimum thickness of 45–50 Å is, as mentioned above, just adequate to reveal both the light and heavy atoms.

The above contrast mechanism is due to the dynamical scattering of electron waves in the crystal. Since the composition of cebaite is close to huanghoite, the multiple scattering process which plays an essential role in the dynamical diffraction in these two crystals will be similar. Hence, it could be expected that the optimum thickness of cebaite is close to that of huanghoite.

Fig. 6 shows the contrast transfer function for spherical aberration coefficients of 0·7 mm and the underfocus values of 300, 400 and 500 Å. Although 500 Å is close to the Scherzer focus (Scherzer, 1949) the image of huanghoite taken at 400 Å underfocus gives a better fit to the atomic structure. It is worth noticing that the spatial frequencies of the strong diffracted beams of cebaite are close to those of huanghoite, which are marked by longer bars in Fig. 6. This may lead to close optimum defocus values for these two minerals.

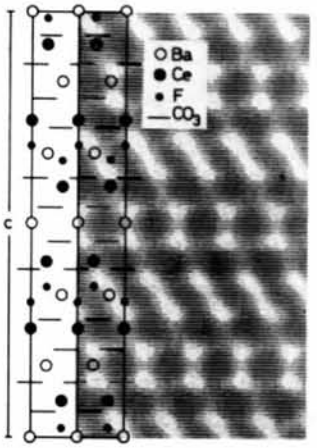

Fig. 5. Structure model and calculated image of huanghoite projected along the *b* axis. Crystal thickness is 63 Å, spherical aberration coefficient 0·7 mm and underfocus 400 Å.

Hence, it is reasonable to assume that huanghoite and cebaite would have close optimum image formation conditions.

6. Determination of the crystal structure of cebaite

Fig. 7(*a*) shows an electron diffraction pattern of cebaite taken with the incident beam parallel to the *b* axis, and Fig. 7(*b*) shows the corresponding electron microscope image inset with the projection of the approximate structure model (marked *A*) and the image of huanghoite (marked *B*) taken under the optimum conditions. It can be seen in Fig. 7(*b*) that, although the white dots in the image of cebaite do not have the same brightness as in the case of huanghoite, their arrangement is quite similar to that of the latter. This is because the basic structure is the same in both minerals. Furthermore, Fig. 7(*b*) shows a good fit between the image and the hypothetical structure model (*A*) if the white dots are interpreted as the region surrounded by columns of atoms as in the case of huanghoite. Therefore, the hypothetical model proposed by Peng & Shen (1979) seems to be correct

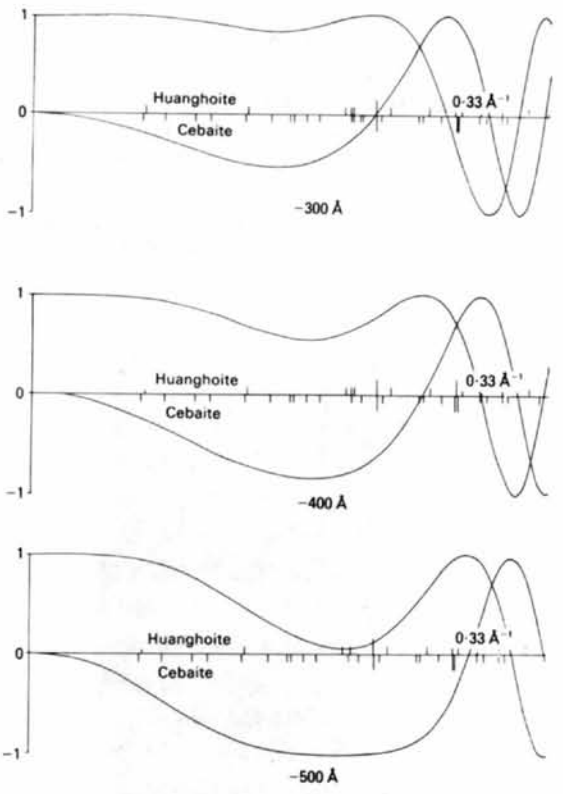

Fig. 6. Contrast transfer function for 100 kV, spherical aberration coefficient 0·7 mm and defocus −300, −400 and −500 Å. Black bars represent the spatial frequencies of diffracted waves of huanghoite (above the abscissa) and cebaite (below the abscissa). Longer bars correspond to the strong beams.

and the image formation condition of the image shown in Fig. 7(*b*) is assumed to be the optimum one.

By referring to the image of cebaite and the crystal structure of huanghoite it is possible to propose some structure model of cebaite, including the positions of the light atoms. It is well established that the symmetry of the structure image reflects the symmetry of the crystal structure projection. According to the previous electron diffraction investigation on cebaite (Li & Fan, 1982*b*), the possible space group of cebaite is $C2$, Cm or $C2/m$. The non-centrosymmetric nature of the image shown in Fig. 7(*b*) indicates that Cm should be the only possible space group of cebaite. However, structure models belonging to different space groups have been proposed for the reason that a slight deviation of the crystal orientation during the exposure time might result in erroneous information about the symmetry. Figs. 8(*a*), (*c*) and (*e*) show the projections of three proposed models. Two of them possess a center of symmetry while the last one does not, because only the last model belongs to the space group Cm.

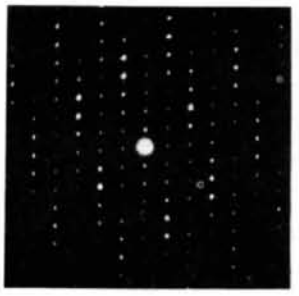

(*a*)

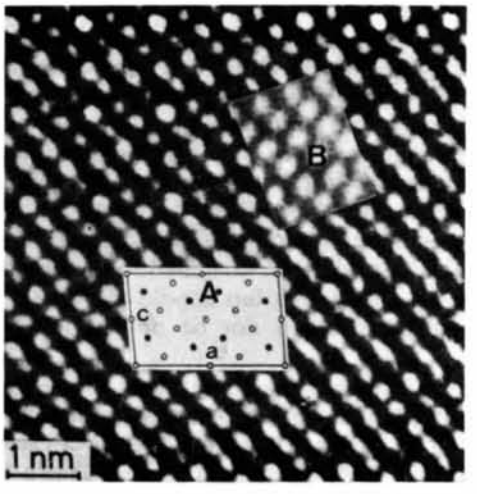

(*b*)

Fig. 7. (*a*) Electron diffraction pattern of cebaite. Incident beam is parallel to the *b* axis. (*b*) Corresponding image of cebaite together with the projected approximate structure model (*A*) and the image of huanghoite (*B*) with thickness 50 Å, taken at 400 Å underfocus.

Table 2. *Observed and calculated intensity of electron diffraction pattern of cebaite for crystal thickness* 100 Å

h0l	I_{obs}	I_c	*h0l*	I_{obs}	I_c	*h0l*	I_{obs}	I_c
001	*m*	8	401	*s*	114	601	*w*	11
200	*w*	6	003	*w*	<1	004	*w*	30
$\bar{2}01$	*w*	3	$\bar{4}02$	*w*	2	403	*s*	185
201	*w*	3	$\bar{2}03$	*m*	20	$\bar{6}02$	*ss*	384
002	*m*	27	402	*ss*	61	$\bar{2}04$	*ss*	600
$\bar{2}02$	*m*	73	203	*w*	12	204	*m*	25
202	*w*	2	600	*w*	9	602	*w*	1
400	*w*	6	$\bar{4}03$	*w*	4	$\bar{4}04$	*w*	25
$\bar{4}01$	*w*	10	$\bar{6}01$	*s*	84	$\bar{6}03$	*ss*	151

Table 3. *Atomic coordinates of cebaite* ($\times 10^3$)

	x	*y*	*z*		*x*	*y*	*z*
Ba(1)	0	0	0	O(1)	110	500	173
Ba(2)	0	500	500	O(2)	398	0	769
Ba(3)	200	500	100	O(3)	216	500	429
Ba(4)	200	0	600	O(4)	292	0	513
Ba(5)	300	500	400	O(5)	309	0	280
Ba(6)	300	0	900	O(6)	191	500	720
				O(7)	41	500	73
Ce(1)	102	0	285	O(8)	98	0	869
Ce(2)	402	500	685	O(9)	492	500	613
Ce(3)	102	500	785	O(10)	16	0	329
Ce(4)	402	0	185	O(11)	21	281	128
				O(12)	487	781	814
F(1)	126	0	117	O(13)	127	281	384
F(2)	426	500	517	O(14)	381	781	558
F(3)	126	500	617	O(15)	220	781	235
F(4)	426	0	17	O(16)	280	281	765
				O(17)	321	281	28
C(1)	51	500	143	O(18)	187	781	914
C(2)	457	0	799	O(19)	427	281	284
C(3)	157	500	399	O(20)	91	781	658
C(4)	351	0	543	O(21)	21	719	128
C(5)	250	0	250	O(22)	487	219	814
C(6)	250	500	750	O(23)	127	719	384
C(7)	351	500	43	O(24)	381	219	558
C(8)	157	0	899	O(25)	220	219	235
C(9)	457	500	299	O(26)	280	719	765
C(10)	51	0	643	O(27)	321	719	28
				O(28)	187	219	914
				O(29)	427	719	284
				O(30)	91	219	658

Owing to the assumption that the optimum crystal thickness and the optimum defocus value of cebaite are close to those of huanghoite, the image simulation has been carried out under several image formation conditions close to the optimum condition for huanghoite. For a thickness of 50 Å and 400 Å underfocus, the calculated images for all the models show regularly arranged white dots (Figs. 8*b*, *d* and *f*), but the image contrast is different. This means that the image taken under the condition close to the assumed optimum one is sensitive to the position of light atoms. The calculated image corresponding to the model belonging to space group Cm is the only one which coincides with the observed image.

Fig. 9 shows the observed image together with the calculated image. A good fit results, not only for the

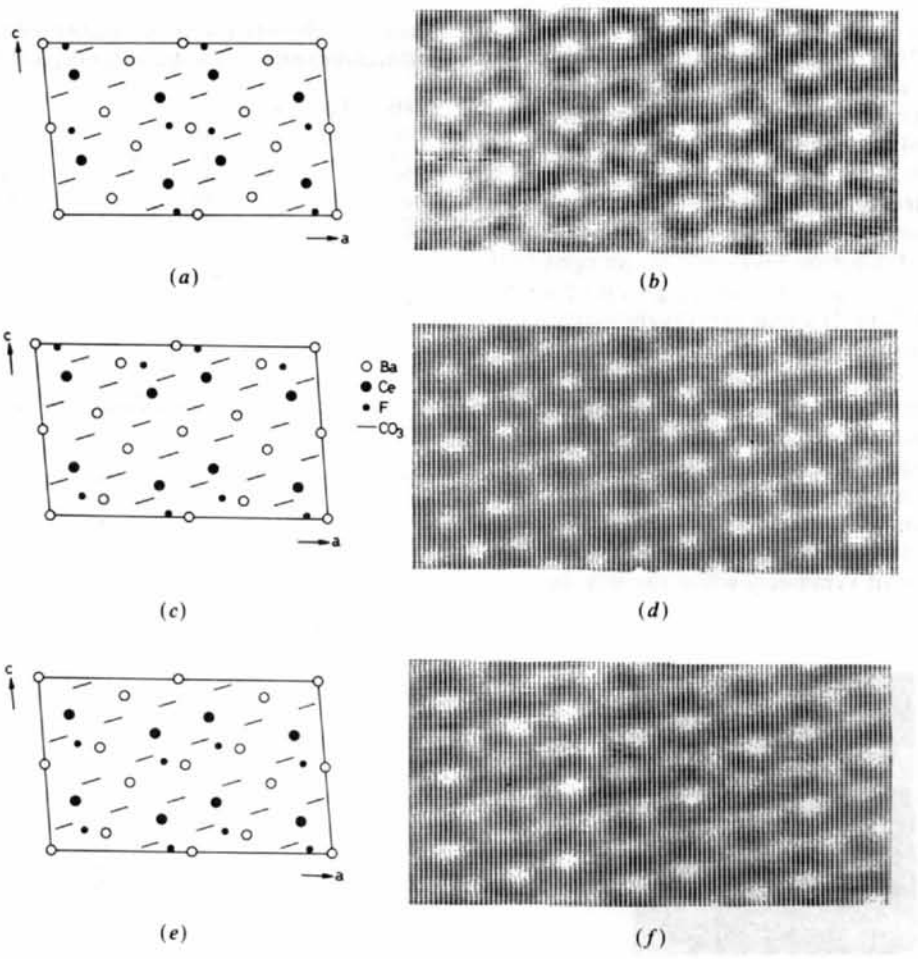

Fig. 8. (*a*), (*c*), (*e*) Projections along the *b* axis of proposed structure models for cebaite. (*a*) and (*c*) have a center of symmetry, but (*e*) does not. (*b*), (*d*), (*f*) Calculated images corresponding to (*a*), (*c*) and (*e*), respectively. Crystal thickness is 50 Å and underfocus value 400 Å.

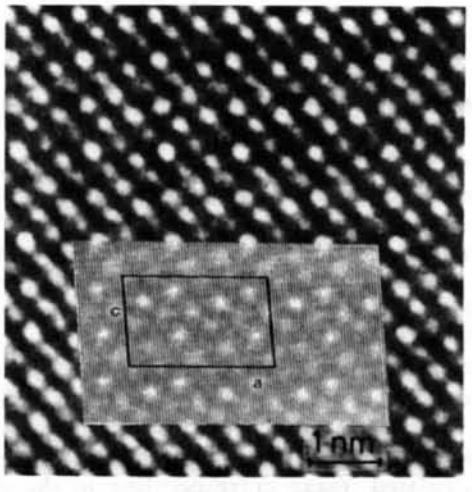

Fig. 9. Observed and calculated images of cebaite. The calculation is carried out assuming the model shown in Fig. 8(*e*). The incident beam is parallel to the *b* axis. Crystal thickness is 50 Å and underfocus 450 Å.

distances between the periodic bright dots but also for their intensity variation, except for the weak diffuse background contrast. Figs. 10(*a*) and (*b*) show the coincidence between the observed and the calculated images for different defocus values. The slight inconsistency on the diffuse background contrast seems to be due to a small misalignment of the specimen crystallite and hence to small differences between the imaging and simulation condition. Such a fairly good agreement could not be obtained for other models.

In Table 2 the observed intensities in the electron diffraction pattern are compared with the intensities calculated by the multislice method for a crystallite of thickness 100 Å. Because the crystal has a wedge shape and the electron diffraction pattern is taken from a region much larger than the imaged area, the crystal thickness of 100 Å is chosen as an average thickness for the intensity calculation. In general, the agreement between the calculated intensities and the observed ones is fairly good. This further confirms

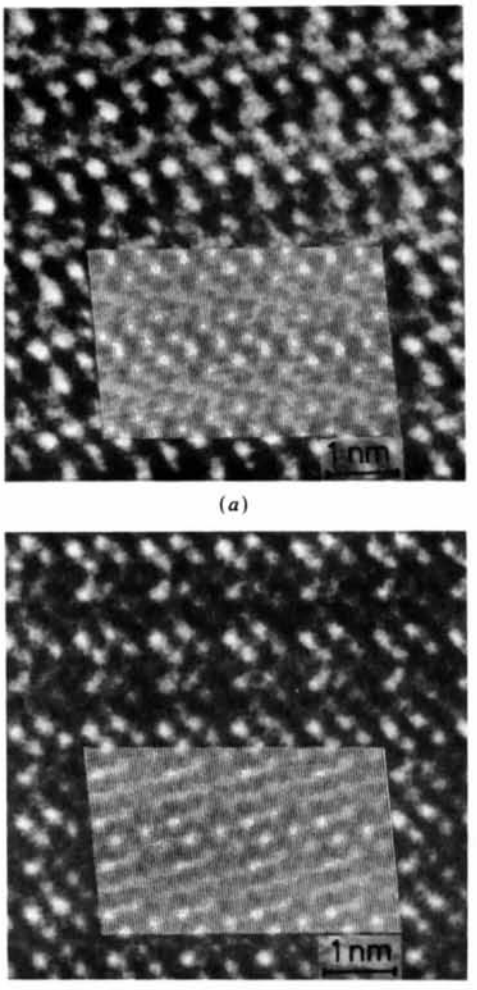

(*a*)

(*b*)

Fig. 10. Observed and calculated images of cebaite. The calculation is carried out assuming the model shown in Fig. 8(*e*). The incident beam is parallel to the *b* axis. Crystal thickness is 50 Å and underfocus (*a*) 200 Å and (*b*) 250 Å.

the proposed model belonging to space group *Cm*. In Table 3 the atomic coordinates of this model are given.

The authors wish to express their gratitude to Professor P. Q. Fu for the valuable mineral samples. Thanks are also due to Assistant Professor H. Endoh, Dr Y. Takai, Messrs N. Ajika, M. Kuwabara, M. Takeda and M. Tomita for their kind help in the calculation and experimental work. FHL would like to thank Professor Z. Z. Peng for constructive discussion.

References

COWLEY, J. M. & IIJIMA, S. (1972). *Z. Naturforsch. Teil A*, **27**, 445–451.

COWLEY, J. M. & MOODIE, A. F. (1957). *Acta Cryst.* **10**, 609–619.

FAN, H. F., ZHANG, R. Y. & ZHAO, G. G. (1963). *Acta Phys. Sin.* **19**, 466–471.

KUMAO, A., HASHIMOTO, H., NISSEN, H.-U. & ENDOH, H. (1981). *Acta Cryst.* A**37**, 229–238.

LI, F. H. & FAN, H. J. (1982*a*). *Acta Phys. Sin.* **31**, 680–684.

LI, F. H. & FAN, H. J. (1982*b*). *Acta Phys. Sin.* **31**, 1206–1214.

LI, F. H., FAN, H. J., YANG, D. Y., FU, P. Q. & KONG, Y. H. (1982). *Acta Phys. Sin.* **31**, 571–576.

LI, F. H., FAN, H. J., ZHANG, P. S. & WANG, Y. H. (1983). *Acta Phys. Sin.* **32**, 460–465.

O'KEEFE, M. A., BUSECK, P. R. & IIJIMA, S. (1978). *Nature (London)*, **274**, 322–324.

PENG, Z. Z. & SHEN, J. C. (1979). *Scientific Papers on Geology for International Exchange Prepared for the International Geological Congress*, pp. 11–18. Beijing, China: Publishing House of Geology.

QIAN, J. Z., FU, P. Q., KONG, Y. H. & GONG, G. H. (1982). *Acta Phys. Sin.* **31**, 577–584.

SCHERZER, O. (1949). *J. Appl. Phys.* **20**, 20–29.

SEMIONOV, E. I. & ZHANG, P. S. (1961). *Kexue Tongbao*, No. 6, pp. 46–48.

SUNDBERG, M. (1978–79). *Chem. Scr.* **14**, 161–166.

TAKAI, Y., HASHIMOTO, H., ENDOH, H. & AJIKA, N. (1981). *EMAG*81, Cambridge, pp. 361–364.

Acta Cryst. (1984). B**40**, 461–465

Structure of the *H* Phase Determined by High-Resolution Electron Microscopy

BY H. Q. YE, D. X. LI AND K. H. KUO

Institute of Metal Research, Academia Sinica, Shenyang, China

(*Received* 27 *January* 1984; *accepted* 18 *May* 1984)

Abstract

A new phase, called *H*, has been found coexisting with the well known σ phase in Fe- and Ni-base superalloys. Owing to an intimate intergrowth of these two phases, a perfect region of *H* never exceeds 10 nm in dimensions. However, its structure was investigated by high-resolution electron microscopy (HREM) and micro electron diffraction and found to be consistent with an interpretation based upon: space group *Cmmm*, $a = 0{\cdot}45$, $b = 1{\cdot}75$, $c = 0{\cdot}45$ nm, $Z = 30$. The atomic positions could easily be fixed owing to the close structure relationship between *H* and σ: $[100]_H \| [4\bar{1}0]_\sigma$, $[010]_H \| [140]_\sigma$, $[001]_H \| [001]_\sigma$.

0108-7681/84/050461-05$01.50